



Synthesis of porous zinc-based/zinc oxide composites via sol–gel and ambient pressure drying routes

Xiao Han¹, Jonathan Harris¹, and Lidija Šiller^{1,*}

¹ School of Chemical Engineering and Advanced Materials, Newcastle University, Newcastle upon Tyne NE1 7RU, UK

Received: 24 October 2017

Accepted: 12 February 2018

Published online:

26 February 2018

© The Author(s) 2018. This article is an open access publication

ABSTRACT

Porous Zn-based and ZnO composites are successfully fabricated via the sol–gel process and ambient pressure drying method using hexane as the drying solvent for the reduction in capillary force during drying process. Various highly porous Zn-based phases (Zn₁-based and Zn₅-based) that are studied by X-ray diffraction analysis, scanning electron microscopy and transmission electron microscopy show that they contribute through heat treatment (at 200 °C) to the development of ambient pressure dried nanoporous wurtzite (hexagonal) ZnO. A macroporous flower-like structure consisting of nanosheets is observed in porous Zn-based composites, and nanoporous structure is observed within platelets of ZnO nanoparticles. Possible routes for preparing highly porous Zn-based/ZnO composites are discovered by detailing the process for ambient pressure drying synthesis of porous wurzite ZnO.

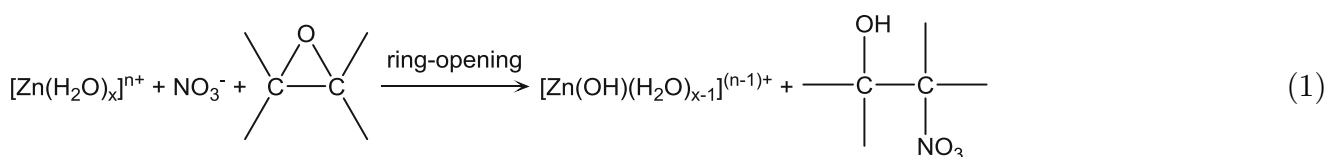
Introduction

Zinc oxide, as a wide band gap semiconductor (with gap energy, $E_g = 3.37$ eV), is known for its dielectric and photocatalytic properties [1, 2]. Zinc oxide can form a variety of stable crystal structures, such as wurtzite and zinblende structures. The tetrahedrally coordinated oxygen in ZnO within the wurtzite (hexagonal) structure gives this material the piezoelectric and pyroelectric properties [3–5]. The pyroelectricity of hexanogal ZnO has been reported in energy application as ‘nanogenerators’ [4]. Until today, the porous ZnO has been synthesised by the

supercritical drying (SCD) method [6–10]. Chen et al. [8] reported that the samples fabricated by SCD method at low temperature (40 °C) are not ZnO unless they are subsequently calcined at 400–500 °C, and their intermediate products are Zn-based (zinc hydroxide nitrate) aerogels. Until now, to the best of our knowledge there is no zinc oxide aerogels prepared via ambient pressure drying (APD) route. The sol–gel process for preparing metal oxide, including ZnO, bases on the hydrolysis with epoxide [11–13]. Synthesis of ZnO nanoparticles with propylene oxide (PPO) has been reported previously [14, 15]. The hydrolysis of zinc salt precursor relies on the acid scavenger (epoxide) through protonation of the

Address correspondence to E-mail: Lidija.Siller@newcastle.ac.uk

epoxide oxygen and subsequent ring opening by the nucleophilic anionic conjugate base [14, 15]. The reaction (1) below illustrates the hydrolysis of aqua zinc nitrate salt with PPO during gelation in order to obtain the ZnO crystal [15].



Supercritical drying (SCD) is a common drying method used to fabricate aerogels. It relies on the extraction of supercritical fluids and requires autoclave to ensure that the solvent in the pores of wet gels reaches the supercritical point. In order to use the SCD method for production of zinc oxide aerogels, including one-step SCD process, a specially designed supercritical drier is required but this introduces additional costs for the manufacturing equipment [16]. The ambient pressure drying (APD) method is an alternative in synthesis of aerogel materials [17–21]. Typically, in APD synthesis of aerogels, an organic solvent with low surface tension is utilised as the drying solvent in order to reduce the capillarity during the drying process [21, 22]. Therefore, the APD method is a more economical process compared to the SCD method and is able to operate continuously as opposed to producing batches [17]. Hexane is a well-known low-surface-tension solvent and it has been often used in the APD synthesis of silica aerogels [18–20, 23]. In this work, we also choose hexane as drying solvent because solvent combination of methanol and hexane has been previously reported in solvent exchange for aerogel preparation [23], and study different phases of porous Zn-based/ZnO composites by APD method of synthesis. The determination of different phases of Zn-based/ZnO composites is necessary in order to develop the APD method of pure ZnO aerogel materials.

Experimental

Preparation of materials

Propylene oxide ($\geq 99.5\%$, PPO), methanol ($\geq 99.9\%$), ethanol ($\geq 99.8\%$), $\text{Zn}(\text{NO}_3)_2 \cdot 6\text{H}_2\text{O}$ (98%)

and hexane ($\geq 98.5\%$) were all purchased from Sigma-Aldrich (UK) and used without any further purification. The initial sol–gel process was carried out via the synthesis method reported for supercritical dried ZnO aerogels [24]. In brief, $\text{Zn}(\text{NO}_3)_2 \cdot 6\text{H}_2\text{O}$ (0.238 g) was mixed with methanol (1.25 ml) and PPO (0.465 g) for gelation in the casting mould (9/11/25 mm of diameter) for 12 h. The formed gels were washed and aged with methanol/ethanol for 5 days. Then, in the following 4 days, the solvent was replaced by hexane 4 times (24 h per time). At the end of the process, the gels were dried at 60–65 °C for 5 h in the water bath and subsequently dried to 100 °C for another 3 h in the oven with air. All the drying processes were carried out under ambient pressure. The obtained Zn-based composites in this work were heated to 200 °C for 2 days to form pure ZnO product. Zn-based (ZBAG) and ZnO (ZOAG) composites were named according to the different conditions of the preparation, as Table 1 indicates. Samples ZBAG1, ZBAG3 and ZBAG4 were prepared under the same conditions except the diameter of their casting mould was 11, 9 and 25 mm, respectively. Samples ZBAG1 and ZBAG2 were prepared under the same conditions except their initial drying temperature was 60 and 65 °C, respectively. Samples ZBAG3 and ZBAG5 were prepared under the same conditions expect the ageing solvents were methanol and ethanol, respectively. Samples ZOAG 1–3 were calcined from samples ZBAG 1–3 at 200 °C.

Table 1 Experimental conditions used for preparing ambient pressure dried porous Zn-based (ZBAG) and ZnO (ZOAG) composites

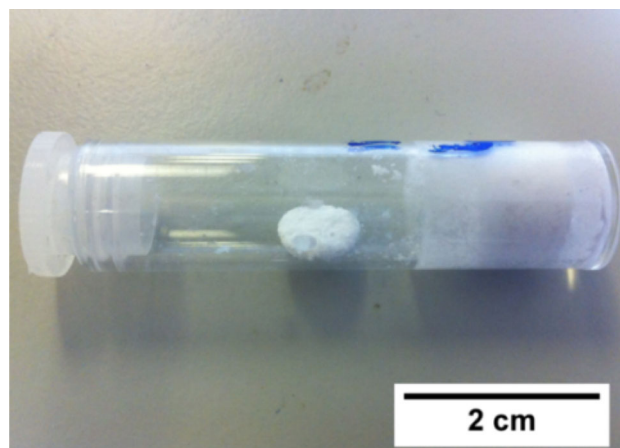
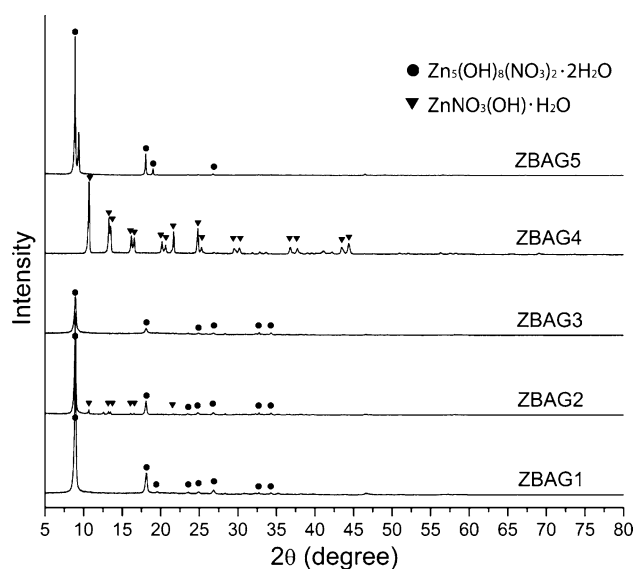
Sample	Diameter of mould (mm)	Ageing solvent	Initial drying temperature (°C)	Heat treatment (°C)
ZBAG1/ZOAG1	11	Methanol	60	200
ZBAG2/ZOAG2	11	Methanol	65	200
ZBAG3/ZOAG3	9	Methanol	60	200
ZBAG4	25	Methanol	60	–
ZBAG5	9	Ethanol	60	–

Materials characterisation

All characterisations have been done at Newcastle University, UK. The PANalytical X'Pert Pro Multipurpose Diffractometer (MPD) is used for X-ray diffraction (XRD) analysis with Cu K α X-rays. All samples were mounted on a silicon low background substrate and scans were done over the 2θ range 5°–120°. FEI XL30 ESEM-FEG (Environmental Scanning Electron Microscope–Field Emission Gun) was used to image the samples in high vacuum mode and 10 keV accelerating voltage. Before SEM imaging, the samples were coated with gold. Philips CM-100 TEM (transmission electron microscope) was used to image samples ZBAG1–3 and ZOAG1–3. The samples for TEM were prepared by ultrasonication of porous Zn-based/ZnO composites in de-ionised water for a prolonged time so that there were no large pieces of samples seen by the eye. The surface area of the samples ZBAG 1 and ZOAG 1 was determined from N₂ adsorption isotherms using a Surfer system (Thermo Scientific). The surface area was calculated by measuring the amount of adsorbed nitrogen gas in a relative vapour pressure of 0.05–0.3 at 77 K by Brunauer–Emmett–Teller (BET) analysis. The conditions of synthesis have been repeated and they lead to the same results (samples ZBAG R1–R3 and R'1–R'3 were repeated under the exact same conditions as samples ZBAG 1–3, and results are shown in supporting information). Fourier transform infrared spectroscopy (FTIR) for ZOAG 1 and ZBAG 1 was analysed by Perkin Elmer Spectrum 2 with a resolution of 4 and 16 scans per sample.

Results and discussion

Porous Zn-based composites are obtained after drying (sample ZBAG 1 is shown in Fig. 1). Figure 2 shows the XRD analysis of ambient pressure dried porous Zn-

**Figure 1** Ambient pressure dried porous Zn-based composites (ZBAG 1).**Figure 2** X-ray diffraction of ambient pressure dried porous Zn-based composites ZBAG1–ZBAG5.

based samples. The diffraction patterns of ZBAG1 are a single phase of Zn₅(OH)₈(NO₃)₂·2H₂O (PDF 01-072-0627) (also called as Zn5) [25–28], and the diffraction

patterns of ZBAG2 are a $\text{Zn}_5(\text{OH})_8(\text{NO}_3)_2 \cdot 2\text{H}_2\text{O}$ phase which coexists with $\text{ZnNO}_3(\text{OH}) \cdot \text{H}_2\text{O}$ (PDF 27-1491) phase (also called as Zn1) [25–28]. Zn₁ and Zn₅ are type I and type IIb crystal structures, respectively, which have been catalogued by Louer et al. based on different lamellar crystal structure [26]. The samples ZBAG1 and ZBAG2 are prepared by the same synthetic method except for the initial drying temperature, and they were dried for 5 h at 60 and 65 °C, respectively. The ZBAG2 samples contain the mixture of porous Zn₅-based and Zn₁-based composites while the ZBAG1 sample only consists of porous Zn₅-based composites. Previous studies suggested that the Zn₁-based and Zn₅-based materials are generated via

hydrolysis at 65 and 60 °C, respectively [25, 27]. Our conventional APD method also fabricates the same distinctive forms of zinc hydroxide nitrate at 65 and 60 °C.

The samples ZBAG1, ZBAG3 and ZBAG4 are prepared by the same synthesis method but with variation of the cross-sectional diameters of casting mould as 11, 9 and 25 mm, respectively. XRD patterns of ZBAG1 and ZBAG3 both show a single phase of $\text{Zn}_5(\text{OH})_8(\text{NO}_3)_2 \cdot 2\text{H}_2\text{O}$ (Zn₅-based), but interestingly the XRD patterns of ZBAG4 show a single phase of $\text{ZnNO}_3(\text{OH}) \cdot \text{H}_2\text{O}$ (Zn₁-based) (Fig. 2). Furthermore, the XRD patterns of ZBAG5 dried with ethanol and 9-mm casting mould reveal a single

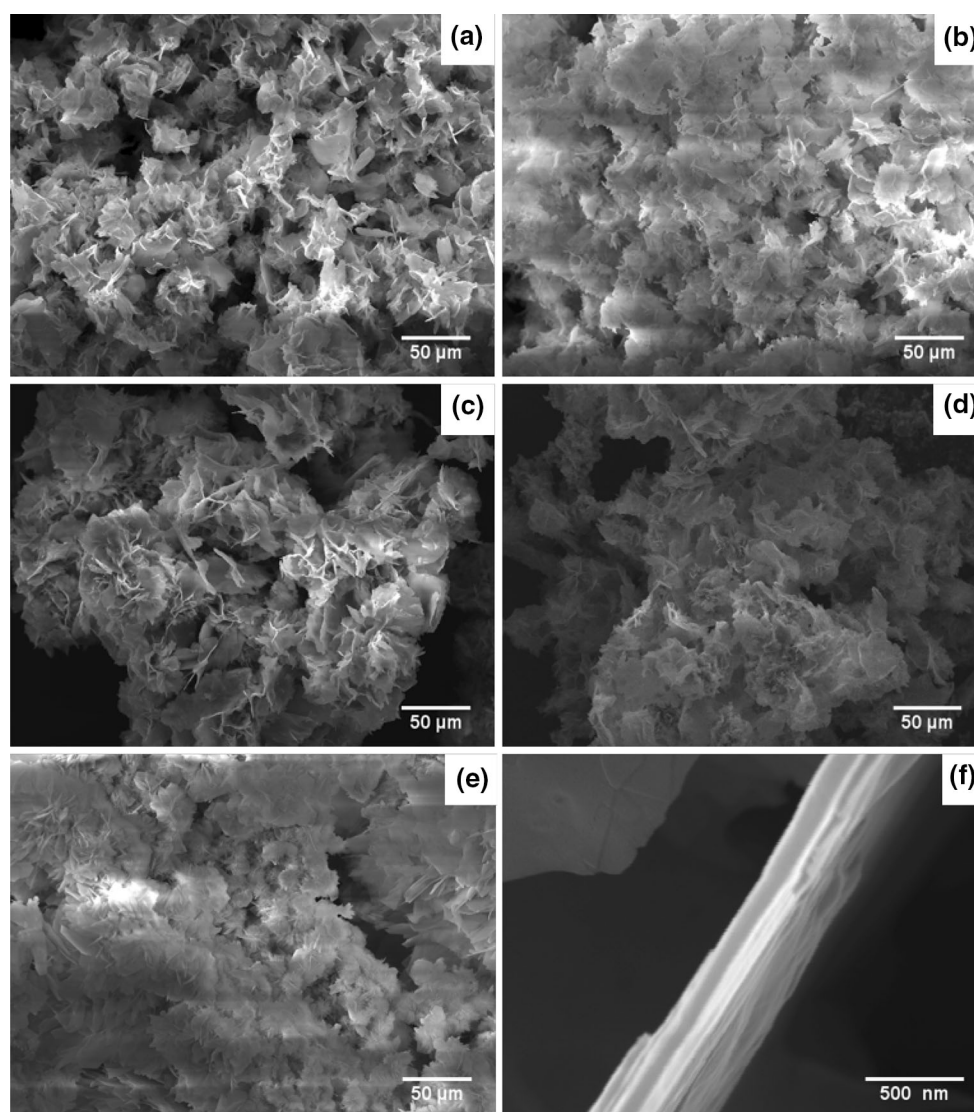


Figure 3 Scanning electron microscope images of ambient pressure dried porous Zn-based composites: **a** ZBAG1, **b** ZBAG2, **c** ZBAG3, **d** ZBAG4, **e** ZBAG5, **f** a captured image of the edge of the vertical nanosheets.

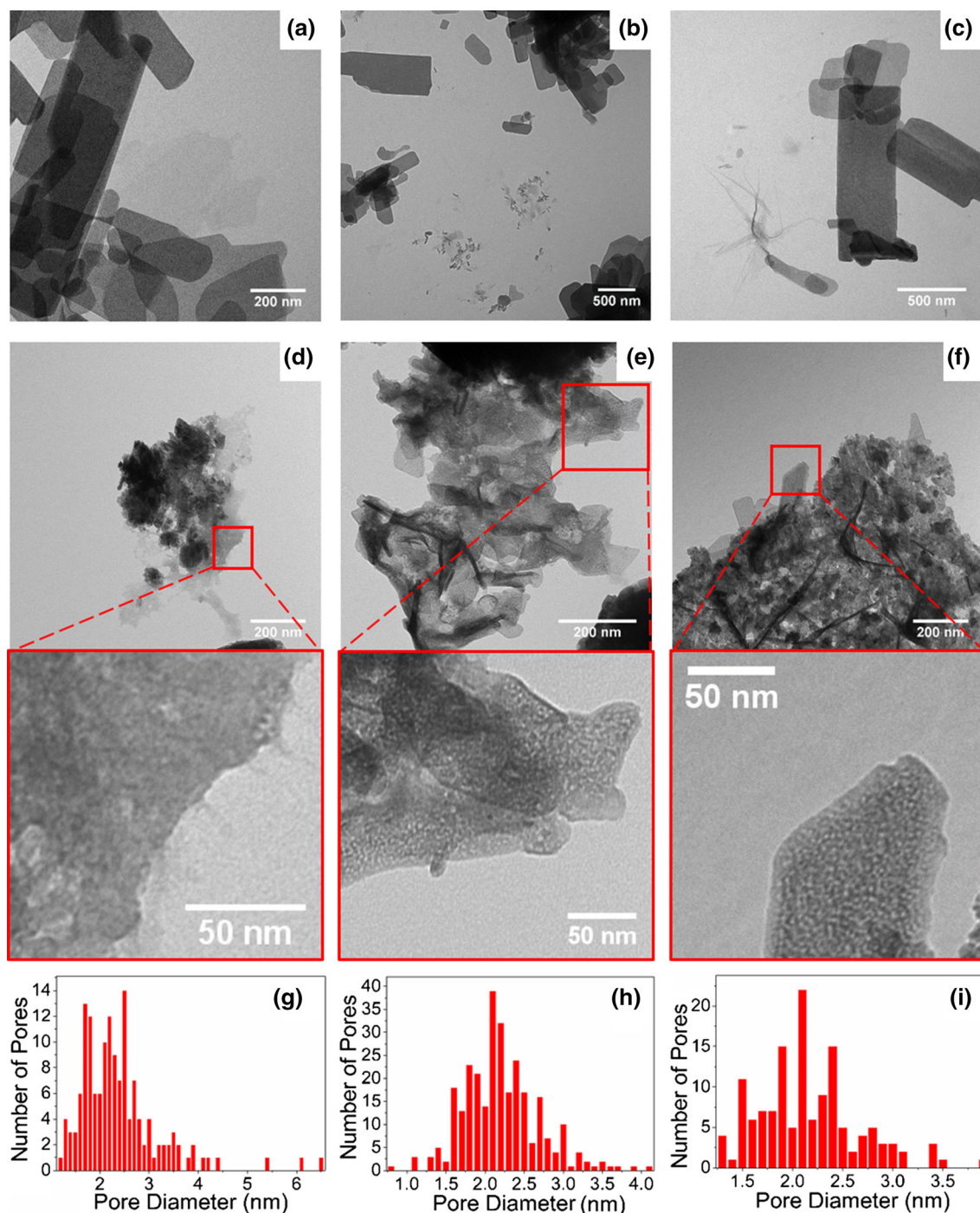


Figure 4 TEM images of zinc-based samples **a** ZBAG 1, **b** ZBAG 2 and **c** ZBAG 3 and zinc oxide samples **d** ZOAG 1, **e** ZOAG 2 and **f** ZOAG 3 and **g–i** the pore sizes distributions of

phase of Zn₅ which is as the same as ZBAG3 (Fig. 2). Therefore, at a given drying temperature, the casting mould affects the formation of Zn-based products because the different evaporation surface area causes a different pressure of the solvent (hexane) inside the

zinc oxide samples 1 (analysed by 149 pores), sample 2 (analysed by 290 pores) and sample 3 (analysed by 138 pores), respectively.

pores of the gels (in the enclosed vials) during the drying process.

All the SEM images of Zn-based samples ZBAG1–5 show a typical flower-like microstructure (Fig. 3a–e) which is previously reported for zinc oxide

nanoparticles and supercritical dried Zn-Co aerogels [29, 30]. Moreover, it has been suggested that this structure gives good stability against the aggregation of the ZnO nanoparticles [31]. Similarly, we suggest that the macroporous (> 50 nm) flower-like structure of our porous Zn-based composites can help prevent capillary shrinkage during the ambient pressure drying process. Figure 3f shows that each plate of porous Zn-based composites is constructed of multi-layered nanosheets. Similarly multi-layered nanosheets are reported in the flower-like ZnO nanoparticles and they are grown upward from the centre [32].

Figure 4a–c shows the TEM images of Zn-based samples ZBAG1–3, respectively. The nanoporous structure can be observed in Fig. 4a. Interestingly, in Fig. 4c, a radial structure is observed. The formation mechanism of the radial structure has previously been discussed in a study of flower-like ZnO nanosheets fabricated with zinc hydroxide carbonate (ZHC) precursor [33]. It has been suggested that the multi-layered nanosheets are caused by the formation of two different surfaces after nucleation of ZHC and proposed that the flower-like structure is formed due to the subsequent self-assembly of those nanosheets [33].

The XRD results of the samples after being heat-treated at 200 °C are presented in Fig. 5. The results show that all the samples ZOAG1–5 contain ZnO (PDF 01-079-0206). ZOAG4 contains also a new phase zinc hydroxide nitrate $\text{Zn}_3(\text{OH})_4(\text{NO}_3)_2$ (PDF 01-070-1361) (Zn_3) which is another type I structure

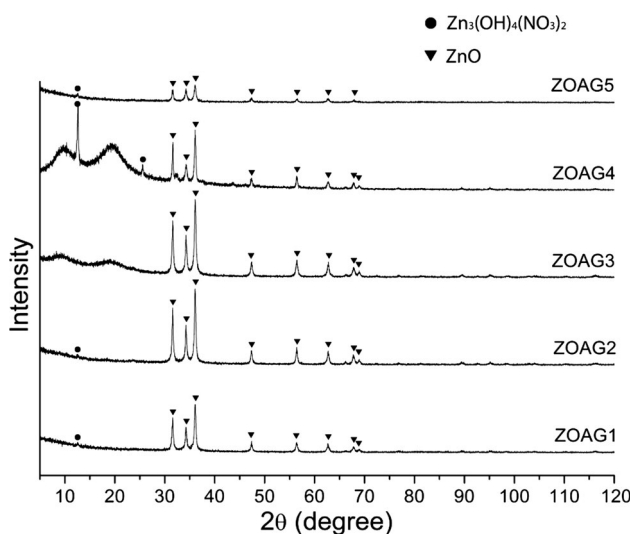


Figure 5 X-ray diffraction of ambient pressure dried porous ZnO composites ZOAG1–ZOAG5.

of zinc hydroxide nitrates. In the XRD patterns of ZOAG4, the most prominent planes are at 12.5° and 25.5° of 2θ and are assigned to (100) and (200) planes of Zn_3 , respectively (PDF 01-070-1361). The samples ZOAG1, ZOAG2 and ZOAG5 have mostly ZnO phase with only a minute amount of Zn_3 phase since only the leading diffraction plane (100) has been observed. In Fig. 5, we see that ZOAG3 has a pure ZnO phase. Therefore, the Zn_3 -based component is an intermediate product which occurs during formation of porous ZnO composites from porous Zn5-based composites and porous Zn1-based composites. Some materials can be directly formed from the sol-gel process without generating any intermediate product during drying such as silica and alumina [18, 22]. However, in this work various porous Zn-based (zinc hydroxide nitrate) composites are obtained by variation of drying conditions. In order to obtain porous ZnO composites, one has to do dehydration of porous Zn-based composites, the samples ZOAG1–3 are obtained from ZBAG1–3 after heat treatment at 200 °C, and they are imaged by TEM (Fig. 4d–f). The nanoplates are observed, but they are much smaller than that of ZBAG samples. The porous structures are also clearly observed in the TEM images of samples ZOAG 1–3 (Fig. 4d–f). The pore sizes distributions analysed by ImageJ of TEM images show the presence of micropores and mesopores (Fig. 4g–i). Comparing TEM images of samples ZOAG 1–3 (Fig. 4d–f) with samples ZBAG 1–3 (Fig. 4a–c), samples ZOAG show that the structure is less ordered, e.g. with shorter range order, the number and size of large rectangular nano-platelets is reduced. Additionally, ZOAG samples are more porous when compared to ZBAG samples. The dehydration of Zn-based nano-platelets induces an extensive microstructure transition with clear nanoporous platelets (Fig. 4g–i) that are assembled within ZnO particles. All pore sizes within the nano-platelets in ZOAG samples are similar, in range 1–3 nm, with maxima at ~ 2 nm in size.

ZnO particles size (L) can be estimated by Scherrer's equation: $L = K \lambda / (B \cos \theta)$, where K is shape factor, B is full width at half maximum (FWHM), λ is X-ray wavelength (0.1542 nm) and θ is diffraction angle. According to Bragg's law, the d spacing can be calculated by expression, $\lambda / 2 \sin \theta$. All our obtained ZnO samples have a wurtzite (hexagonal) crystal structure (PDF 01-079-0206). Therefore, the lattice parameters have a relation with d spacing as $(1/$

$d^2 = 4(h^2 + k^2 + hk)/3a^2 + l^2/c^2$. The XRD patterns of sample ZOAG1 have peaks with 2θ values of 47.36° , 56.40° and 62.66° corresponding to (102), (110) and (103) planes and FWHM values of 0.34, 0.40 and 0.43, by Scherrer's equation, giving the particles sizes of 25.53, 22.55 and 21.65 nm, respectively. Therefore, an average size of ZnO can be estimated to be 23.2 nm. According to Bragg's law, the d spacing is $d(102) = 0.192$ nm and $d(110) = 0.163$ nm. From planes (102) and (110), the lattice parameters of sample ZOAG1 were calculated by the relation of the lattice parameters as $a = b = 0.326$ nm and $c = 0.524$ nm. Similarly as above, samples ZOAG2 and ZOAG3 have average sizes, 26.0 and 21.3 nm, respectively. The lattice parameters of ZOAG2 and ZOAG3 are all $a = b = 0.326$ nm and $c = 0.524$ nm. Samples ZOAG 1–3 have a same ratio of lattice parameters c/a to be 1.607 which is close to the ideal hexagonal unit cell ($c/a = 1.633$), and the Zn–O length calculated from geometry of the ZnO wurtzite crystal structure is 0.1986 nm. Interestingly, porous ZnO samples with wurzite (hexagonal) crystal structure are promising materials in energy applications, due to their pyroelectric properties [4].

In order to study the chemical composition of the products, samples ZBAG1 and ZOAG1 were characterised by FTIR. The FTIR spectrum of sample ZBAG1 (Fig. 6) shows a broad band around 3300 cm^{-1} and a peak around 1630 cm^{-1} that corresponds to O–H stretching and H–O–H bending of $\text{Zn}_5(\text{OH})_8(\text{NO}_3)_2 \cdot 2\text{H}_2\text{O}$, respectively [34], and further band at $\sim 1363\text{ cm}^{-1}$ corresponds to NO_3 vibrations in Zn– NO_3 [35]. The FTIR spectrum of sample ZOAG1 shows the most prominent band is observed in energy range $400\text{--}500\text{ cm}^{-1}$, which corresponds to

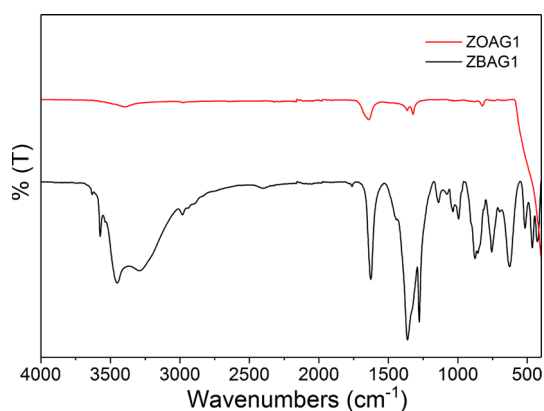


Figure 6 FTIR of samples ZBAG1 and AOZG1.

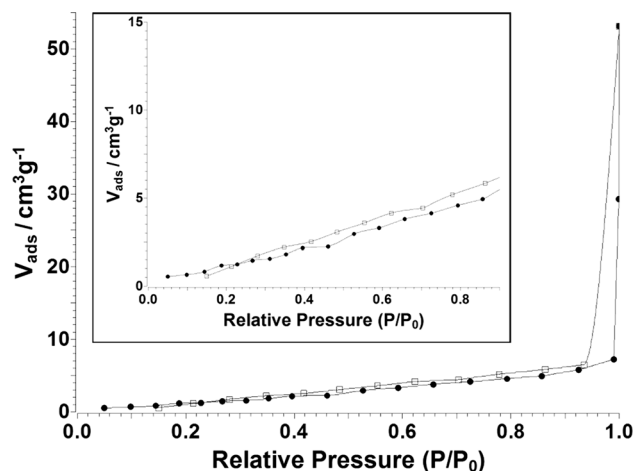
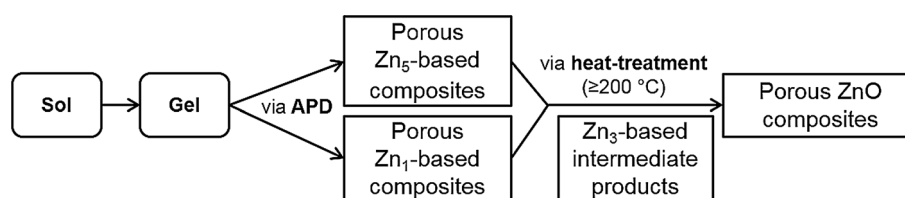


Figure 7 Nitrogen adsorption–desorption isotherm of sample ZBAG 1.

Zn–O stretch [36]. In addition, comparing the FTIR spectrum of ZOAG1 with that of ZBAG1, there is absence/weakness of peaks observed in ZBAG1 sample over all energy range; therefore, this confirms the phase transition from $\text{Zn}_5(\text{OH})_8(\text{NO}_3)_2 \cdot 2\text{H}_2\text{O}$ to ZnO upon heat treatment. The successful fabrication and purity of ZnO via our APD method is comparable to SCD method published in the literature [4, 5] showing advantages in manufacturing process with reduced equipment requirements.

The ZBAG 1 sample, which has the single phase of porous Zn₅-based product, was also characterised by nitrogen gas adsorption and desorption isotherm at 77 K (Fig. 7). According to the classification of isotherm types determined by the International Union of Pure and Applied Chemistry (IUPAC), a standard type VI isotherm is identified, and it represents a typical macroporous material with highly uniform surfaces [37]. This is in agreement with the flower-like macroporous architecture revealed in Fig. 3a–e which consists of large rectangular nanosheets (Fig. 4a–c). The surface area of ZBAG 1 is $7.26\text{ m}^2/\text{g}$ which also verifies the macroporous structure of the sample. The surface area of ZOAG 1 is $11.80\text{ m}^2/\text{g}$, showing increase in surface area upon heating. We suggest that the increase in surface area from porous Zn-based composites to porous ZnO composites is caused by the change of microstructure as observed by the transmission electron microscope images, as comparison between Fig. 4a–f. It is known [38] that if the pore size is very small or comparable with diameter of adsorptive molecules used in isotherm adsorption measurements, surface areas will be

Figure 8 Schematic diagram of ambient pressure drying routes of porous Zn-based/ZnO composites.



unreliable and can be underestimated. Possible reasons are [38]: (1) that there is a different density of adsorbed molecules during pore filling, in small pores comparing to usual liquid phase, which is known to be used as standard input parameter in adsorption isotherm analysis method (such as BET); (2) the roughness of the materials cage containing the pores with pore shapes influencing the adsorption; (3) changes in effective cross-sectional area of adsorptive molecules. In case of N_2 , N_2 has also a quadrupole moment, so the electrostatic repulsion of N_2 with ZnO/Zn-based cages during adsorption process within the small pores (< 2 nm) may give underestimated surface area of the material.

Finally, the majority of porous planes are self-assembled in stacks to form flower-like microstructure (Fig. 3f), so the diffusion of nitrogen into the stack of porous planes during N_2 adsorption experiment may be hindered, which would give an underestimate of the sample surface area. Further study of adsorption of different adsorptive molecules (such as argon, CO_2) at different temperatures and with different methods is required, to understand pore adsorption and pore size distribution and distinguish above-mentioned phenomena.

In APD synthesis in this work, porous ZnO composites can be only obtained after additional heat treatment after the initial synthesis of porous Zn-based composites is completed. Therefore, it is essential to know the components of the materials at each stage for the APD synthesis. We suggest a process presented in Fig. 8 for control and design of the APD synthesis of porous Zn-based/ZnO composites.

Conclusions

Porous Zn-based and ZnO composites are successfully fabricated via the sol–gel process and ambient pressure drying route. The variations of phases are identified by the XRD analysis. When porous Zn-based composites are obtained, high drying temperature (200 °C) and large casting mould size are required to obtain Zn_1 -based samples. Alternatively, low drying

temperature and small casting mould size are required for Zn_5 -based samples. Morphologies of different phases are studied by SEM and TEM. A macroporous flower-like structure containing the nanosheets is observed in Zn-based products by SEM imaging. Micropores and mesopores in ZnO aerogels are observed in the TEM images. This work reports conditions necessary for the ambient pressure dried ZnO porous materials and may be important for future synthesis of ZnO porous material composites (with silica, alumina, etc.) using the APD method. The APD synthesis proposed has low energy requirements (only heating at 200 °C at atmospheric pressure) and does not require expensive equipment as in SCD.

Acknowledgements

The author Dr. Xiao Han wishes to thank Newcastle University for the award of a Teaching Studentship. We would also like to thank to EPSRC (Grant No. EP/R000131/1) and to EPSRC/BEIS funding bodies for a partial financial support (Grant No. EP/R021503/1).

Electronic supplementary material: The online version of this article (<https://doi.org/10.1007/s10853-018-2138-2>) contains supplementary material, which is available to authorized users.

Open Access This article is distributed under the terms of the Creative Commons Attribution 4.0 International License (<http://creativecommons.org/licenses/by/4.0/>), which permits unrestricted use, distribution, and reproduction in any medium, provided you give appropriate credit to the original author(s) and the source, provide a link to the Creative Commons license, and indicate if changes were made.

References

- [1] Tian ZR et al (2003) Complex and oriented ZnO nanostructures. *Nat Mater* 2(12):821–826

- [2] Carcia PF, McLean RS, Reilly MH (2006) High-performance ZnO thin-film transistors on gate dielectrics grown by atomic layer deposition. *Appl Phys Lett* 88(12):123509
- [3] Zhong Lin W (2004) Zinc oxide nanostructures: growth, properties and applications. *J Phys Condens Matter* 16(25):R829
- [4] Yang Y et al (2012) Pyroelectric nanogenerators for harvesting thermoelectric energy. *Nano Lett* 12(6):2833–2838
- [5] Bowen CR et al (2014) Pyroelectric materials and devices for energy harvesting applications. *Energy Environ Sci* 7(12):3836–3856
- [6] Krumm M, Pueyo CL, Polarz S (2010) Monolithic zinc oxide aerogels from organometallic sol–gel precursors. *Chem Mater* 22(18):5129–5136
- [7] El Ghouli J, Barthou C, El Mir L (2012) Synthesis, structural and optical properties of nanocrystalline vanadium doped zinc oxide aerogel. *Physica E* 44(9):1910–1915
- [8] Chen B et al (2013) Monolithic zinc oxide aerogel with the building block of nanoscale crystalline particle. *J Porous Mater* 20(5):1051–1057
- [9] Meddouri M et al (2014) Effect of co-solvent on structural and morphological properties of ZnO aerogel prepared by a modified sol–gel process. *Eur Phys J Appl Phys* 66(01):10402
- [10] Wang P et al (2014) Zinc oxide aerogel-like materials with an intriguing interwoven hollow-sphere morphology for selective ethanol sensing. *RSC Adv* 4(42):21815–21818
- [11] Baumann TF et al (2005) Synthesis of high-surface-area alumina aerogels without the use of alkoxide precursors. *Chem Mater* 17(2):395–401
- [12] Gan L et al (2005) Synthesis of alumina aerogels by ambient drying method and control of their structures. *J Porous Mater* 12(4):317–321
- [13] Tokudome Y et al (2007) Synthesis of monolithic Al_2O_3 with well-defined macropores and mesostructured skeletons via the sol–gel process accompanied by phase separation. *Chem Mater* 19(14):3393–3398
- [14] Gash AE et al (2001) Use of epoxides in the sol–gel synthesis of porous iron(III) oxide monoliths from Fe(III) salts. *Chem Mater* 13(3):999–1007
- [15] Cui H, Zayat M, Levy D (2005) Sol–gel synthesis of nanoscaled spinels using propylene oxide as a gelation agent. *J Sol-Gel Sci Technol* 35(3):175–181
- [16] Aegerter MA, Leventis N, Koebel MM (2011) *Aerogels handbook*. Springer, Berlin
- [17] Prakash SS et al (1995) Silica aerogel films prepared at ambient-pressure by using surface derivatization to induce reversible drying shrinkage. *Nature* 374:439–443
- [18] Prakash SS, Brinker CJ, Hurd AJ (1995) Silica aerogel films at ambient-pressure. *J Non-Cryst Solids* 190(3):264–275
- [19] Rao AP, Rao AV, Pajonk GM (2007) Hydrophobic and physical properties of the ambient pressure dried silica aerogels with sodium silicate precursor using various surface modification agents. *Appl Surf Sci* 253(14):6032–6040
- [20] Wei TY et al (2007) Preparation of monolithic silica aerogel of low thermal conductivity by ambient pressure drying. *J Am Ceram Soc* 90(7):2003–2007
- [21] Shlyakhtina A, Oh YJ (2008) Transparent SiO_2 aerogels prepared by ambient pressure drying with ternary azeotropes as components of pore fluid. *J Non-Cryst Solids* 354(15–16):1633–1642
- [22] Wu L et al (2010) Fabrication of hydrophobic alumina aerogel monoliths by surface modification and ambient pressure drying. *Appl Surf Sci* 256(20):5973–5977
- [23] Uzma KHB, Rao AV, Rao AP (2008) A new route for preparation of sodium-silicate-based hydrophobic silica aerogels via ambient-pressure drying. *Sci Technol Adv Mater* 9(3):035006
- [24] Gao YP, Sisk CN, Hope-Weeks LJ (2007) A sol–gel route to synthesize monolithic zinc oxide aerogels. *Chem Mater* 19(24):6007–6011
- [25] Stahlin W, Oswald HR (1970) The crystal structure of zinc hydroxide nitrate, $\text{Zn}_5(\text{OH})_8(\text{NO}_3)_2 \cdot 2\text{H}_2\text{O}$. *Acta Crystallogr Sect B* 26(6):860–863
- [26] Louer M, Louer D, Grandjean D (1973) Etude structurale des hydroxynitrates de nickel et de zinc. I. Classification structurale. *Acta Crystallogr Sect B* 29(8):1696–1703
- [27] Eriksson L, Louer D, Werner PE (1989) Crystal structure determination and rietveld refinement of $\text{Zn}(\text{OH})(\text{NO}_3) \cdot \text{H}_2\text{O}$. *J Solid State Chem* 81(1):9–20
- [28] Chouillet C et al (2004) Characterization of zinc hydroxynitrates by diffuse reflectance infrared spectroscopy—structural modifications during thermal treatment. *Spectrochim Acta A Mol Biomol Spectrosc* 60(3):505–511
- [29] Li B, Wang Y (2009) Facile synthesis and enhanced photocatalytic performance of flower-like ZnO hierarchical microstructures. *J Phys Chem C* 114(2):890–896
- [30] Davis M et al (2012) Tailoring cobalt doped zinc oxide nanocrystals with high capacitance activity: factors affecting structure and surface morphology. *RSC Adv* 2(5):2061–2066
- [31] Zhao X et al (2014) Sol–gel-based hydrothermal method for the synthesis of 3D flower-like ZnO microstructures composed of nanosheets for photocatalytic applications. *Ceram Int* 40(4):5507–5514
- [32] Adhyapak PV et al (2014) Structurally enhanced photocatalytic activity of flower-like ZnO synthesized by PEG-assisted hydrothermal route. *Ceram Int* 40(1, Part B):1951–1959
- [33] Li J, Fan H, Jia X (2010) Multilayered ZnO nanosheets with 3D porous architectures: synthesis and gas sensing application. *J Phys Chem C* 114(35):14684–14691

- [34] Nityashree N, Rajamathi M (2013) Interstratified composite of the anionic clays, $Zn_5(OH)_8(NO_3)_2 \cdot 2H_2O$ and $Ni_3Zn_2(OH)_8(NO_3)_2 \cdot 2H_2O$, by delamination-costacking. *J Phys Chem Solids* 74(8):1164–1168
- [35] Bull RMR et al (2011) Hydroxy double salts as versatile storage and delivery matrices. *J Mater Chem* 21(6):1822–1828
- [36] Sadollahkhani A et al (2014) Synthesis, structural characterization and photocatalytic application of $ZnO@ZnS$ core-shell nanoparticles. *RSC Adv* 4(70):36940–36950
- [37] Thommes M et al (2015) Physisorption of gases, with special reference to the evaluation of surface area and pore size distribution (IUPAC Technical Report). *Pure Appl Chem* 87:1051–1069
- [38] Carrott MMLR et al (2001) Adsorption of nitrogen, neopentane, n-hexane, benzene and methanol for the evaluation of pore sizes in silica grades of MCM-41. *Microporous Mesoporous Mater* 47(2):323–337